Angular-Shaped 4,9-Dialkyl α- and β-Naphthodithiophene-Based Donor–Acceptor Copolymers: Investigation of Isomeric Structural Effects on Molecular Properties and Performance of Field-Effect Transistors and Photovoltaics

Sheng-Wen Cheng, De-Yang Chiou, Che-En Tsai, Wei-Wei Liang, Yu-Ying Lai, Jhih-Yang Hsu, Chain-Shu Hsu, Itaru Osaka, Kazuo Takimiya, and Yen-Ju Cheng**

Two angular-shaped 4,9-didodecyl α-aNDT and 4,9-didodecyl β-aNDT isomeric structures have been regiospecifically designed and synthesized. The distannylated α-aNDT and β-aNDT monomers are copolymerized with the Br-DTNT monomer by the Stille coupling to furnish two isomeric copolymers, PαNDTDTNT and PβNDTDTNT, respectively. The geometric shape and coplanarity of the isomeric α-aNDT and β-aNDT segments in the polymers play a decisive role in determining their macroscopic device performance. Theoretical calculations show that PαNDTDTNT possesses more linear polymeric backbone and higher coplanarity than PβNDTDTNT. The less curved conjugated main chain facilitates stronger intermolecular π–π interactions, resulting in more redshifted absorption spectra of PαNDTDTNT in both solution and thin film compared to the PβNDTDTNT counterpart. 2D wide-angle X-ray diffraction analysis reveals that PαNDTDTNT has more ordered π-stacking and lamellar stacking than PβNDTDTNT as a result of the lesser curvature of the PαNDTDTNT backbone. Consistently, PαNDTDTNT exhibits a greater field effect transistor hole mobility of 0.214 $cm^2 V^{-1} s^{-1}$ than PβNDTDTNT with a mobility of 0.038 $cm^2 V^{-1} s^{-1}$. More significantly, the solar cell device incorporating the PαNDTDTNT:$PC_{71}BM$ blend delivers a superior power conversion efficiency (PCE) of 8.01% that outperforms the PβNDTDTNT:$PC_{71}BM$-based device with a moderate PCE of 3.6%.

1. Introduction

Organic photovoltaics (OPVs) and organic field effect transistors (OFETs) have attracted much interest over the past decade. Conjugated polymers are an important class of organic materials in terms of tunable molecular properties and easy solution-processability.[1] One of the important criteria of acquiring high-performance-conjugated polymers is to induce strong π–π stacking and ordered structure that facilitate charge transportation between intermolecular polymer chains.[2] Müllen and co-workers demonstrated that the backbone curvature of the polymers plays an important role in determining molecular packing and their charge carrier mobilities.[3] In general, the curvature of backbone is governed by the molecular geometry and symmetry of the conjugated segments in the polymers. The polymer with wavy backbone results in lesser ordered packing structure and thus lower mobility. Recently, Hou and co-workers demonstrated that the benzodithiophene (BDT)-based polymer with more linear conformation results in more ordered interchain packing in thin film and better photovoltaic performance.[4] Similar observations were also found in the isoindigo-based D-A copolymers reported by Pei and co-workers.[5] In addition to the main-chain configuration, side-chain engineering also has an equally important impact. The placement of aliphatic side chains on a polymer backbone also significantly influences the backbone conformations as well as interchain interactions which in turn determine the molecular packing, crystallinity, and thereby charge transportation properties.[6]

Despite that numerous π-conjugated electron-rich donors and electron-deficient acceptors have been developed, only a few donor building blocks such as BDT have successfully led to the high-efficiency donor–acceptor-conjugated copolymers for OPVs applications.[7] Along with the widely used tricyclic BDT that is the shortest member among the acenedithiophene family, an extended tetracyclic naphthodithiophene (NDT), where two thiophene units are fused with a central naphthalene unit, emerges as a promising donor building block.[8] Depending on the structural geometry, the NDT derivatives are primarily categorized into linear-shaped NDT (lNDT)[9] and angular-shaped NDT (aNDT) isomers.[10] The aNDT can

S.-W. Cheng, D.-Y. Chiou, C.-E. Tsai, W.-W. Liang, Dr. Y.-Y. Lai, J.-Y. Hsu, Prof. C.-S. Hsu, Prof. Y.-J. Cheng
Department of Applied Chemistry
National Chiao Tung University
1001 University Road Hsin-Chu 30010, Taiwan
E-mail: yjcheng@mail.nctu.edu.tw

Dr. I. Osaka, Prof. K. Takimiya
Emergent Molecular Function Research Group
RIKEN Center for Emergent Matter Science
Wako, Saitama 351-0198, Japan
E-mail: takimiya@riken.jp

DOI: 10.1002/adfm.201502338

be further classified into another two isomeric structures denoted as α-aNDT and β-aNDT where the sulfur atoms of the thiophene units are attached on the α- and β-position of the central naphthalene unit, respectively. Takimiya et al. have demonstrated that the α-aNDT-based copolymer has more linear polymer backbone (pseudostraight) than the corresponding lNDT-based counterpart,[10d] thereby resulting in the more ordered crystalline structure and higher mobility. To fully exploit the aNDT-based polymers, incorporation of aliphatic side chains onto the aNDT units is essential to improve solubility of the resultant copolymers. Takimiya et al. and Osaka et al. first reported the synthesis of 5,10-dialkyl α-aNDT[11] unit and its corresponding donor–acceptor copolymer with superior solar cell performance.[8c]

On account of the aforementioned considerations, it is of great interest to design new aNDT derivatives by implementing molecular engineering in two aspects: (1) shifting the aliphatic side chains from the outer 5,10-positions to the inner 4,9-positions, (2) changing the isomeric main chain structure from the α-form to the β-form. Cheng et al. developed a facile synthetic strategy that can regiospecifically synthesize angular 4,9-dialkylated α-aNDT as well as 4,9-dialkylated β-aNDT.[12] Two isomeric dithienyl-ene-diyne intermediates undergo base-induced 6π-cyclizations to construct the central naphthalene cores of the 4,9-didodecyl-α-aNDT and 4,9-didodecyl-β-aNDT, respectively (**Figure 1**).

Compared with the commonly used 2,1,3-benzothiadiazole (BT), naphtho[1,2-*c*:5,6-*c*]bis[1,2,5]thiadiazole (NT),[13] a doubly BT-fused heterocycle, is a superior acceptor due to its stronger electron-withdrawing ability and the more π-extended structure. The centrosymmetric NT with a C2h symmetry can lead to more straight backbone when combined with centrosymmetric units, compared to the corresponding polymer with axisymmetric BT with a C2v symmetry, resulting in better polymer chain ordering.[13c] In this research, the two isomeric 4,9-didodecyl α-aNDT and 4,9-didodecyl β-aNDT monomers were copolymerized with an NT-containing monomer, dithienyl naphthobisthiadiazole (DTNT), to generate PαNDTDTNT and PβNDTDTNT, respectively. The two isomeric α-aNDT- and β-aNDT-based copolymers provide us with an ideal system to investigate the electronic and steric influences on the microscopic properties such as absorption, electrochemical, polymeric curvature, and molecular packing that ultimately govern the macroscopic characteristics of OFETs and OPVs.

2. Results and Discussion

2.1. Synthesis and Thermal Properties of the Polymers

Synthetic routes of the monomers Sn-α-aNDT and Sn-β-aNDT are shown in **Scheme 1**. Olefination of 3-bromothiophene-2-carbaldehyde (**1**) and 2-bromothiophene-3-carbaldehyde (**4**) by McMurry coupling reactions furnished the (*E*)-1,2-bis(3-bromothiophen-2-yl)ethene (**2**) and (*E*)-1,2-bis(2-bromothiophen-3-yl)ethene (**5**), respectively. The dithiophenyl-ene-diyne (**3**) and (**6**) were synthesized by the Sonogashira coupling reactions of (**2**) and (**5**) with tetradec-1-yne in good yields, respectively. The 1,8-Diazabicycloundec-7-ene (DBU) induced tandem 6π-cyclizations of (**3**) and (**6**) resulted in the formation of the central naphthalene units with the dodecyl groups regiospecifically at the 4,9-positions of the α-aNDT and β-aNDT units. Subsequently, the Sn-α-aNDT and Sn-β-aNDT monomers were obtained by the lithiations of α-aNDT and β-aNDT followed by quenching with trimethyltin chloride. The two monomers were copolymerized with the Br-DTNT[13] monomer by the Stille coupling to afford PαNDTDTNT and PβNDTDTNT, respectively (Scheme 1).

The molecular weight was determined to be M_n = 67.3 kDa with a polydispersity index (PDI) of 1.3 for PαNDTDTNT, and M_n = 28.3 kDa with a PDI of 2.1 for PβNDTDTNT by gel permeation chromatography (GPC) measurements (**Table 1**). PβNDTDTNT is soluble well in tetrahydrofuran (THF) at room temperature, whereas PαNDTDTNT is partially soluble in THF and can be dissolved in warm chlorobenzene (CB) or *ortho*-dichlorobenzene (oDCB), implying that PαNDTDTNT has stronger intermolecular interactions. The thermal properties of the polymers were evaluated by thermogravimetric analysis (TGA) and differential scanning calorimetry (DSC). Both of the

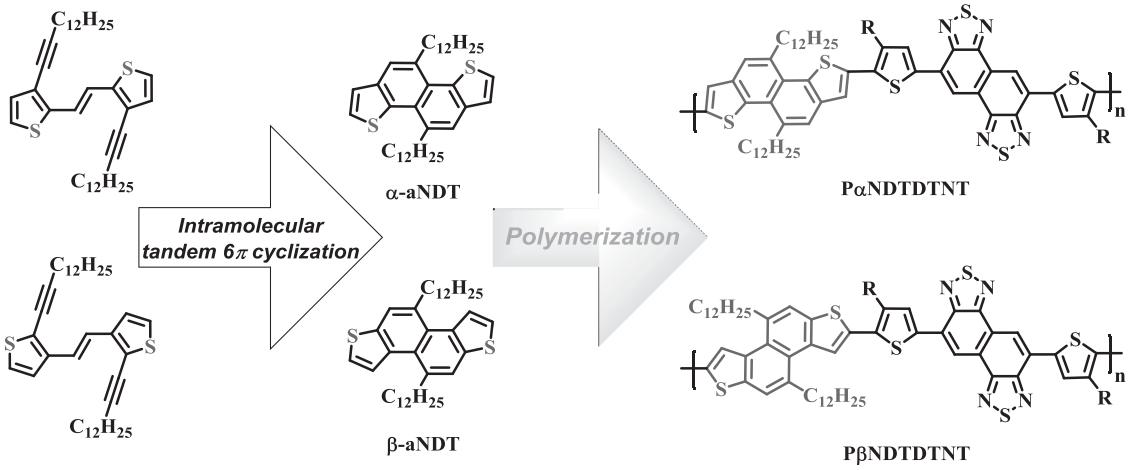

Figure 1. The chemical structures of α-aNDT, β-aNDT, PαNDTDTNT, and PβNDTDTNT copolymers.

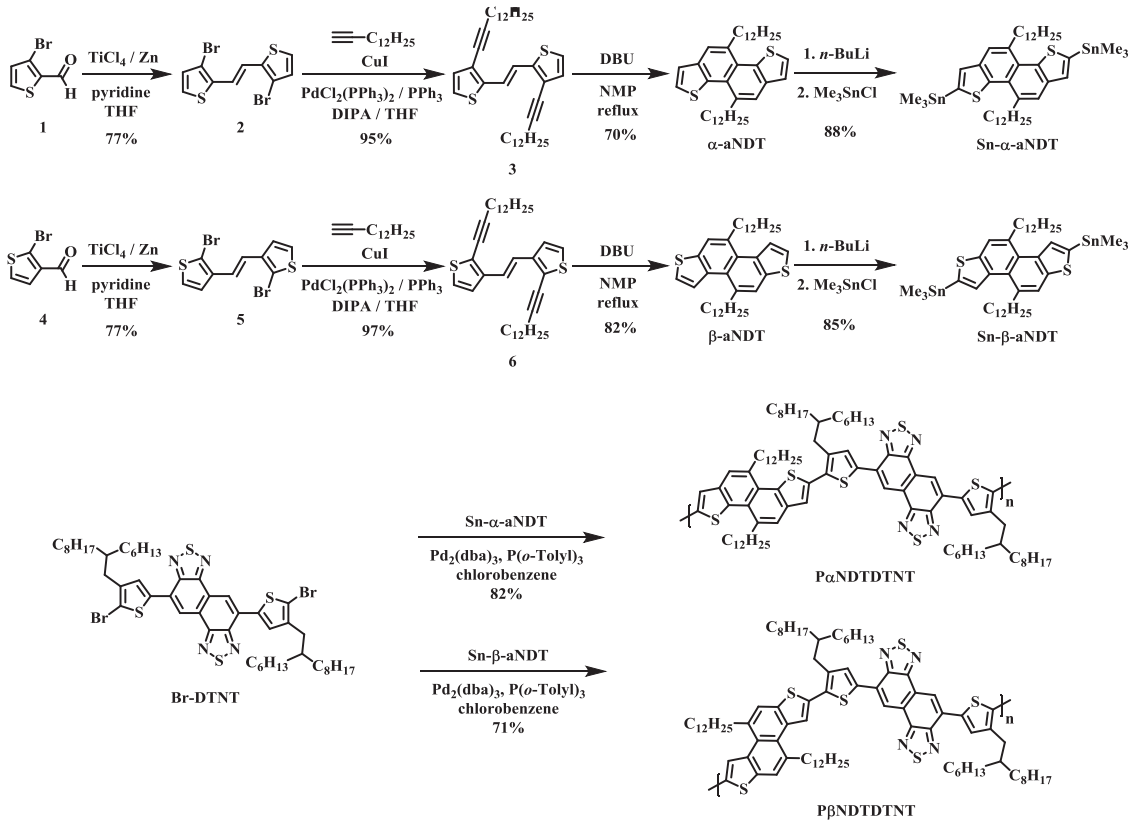

Scheme 1. Synthetic routes for α-aNDT and β-aNDT and their corresponding copolymers.

polymers showed sufficiently high decomposition temperatures (T_d) of 446 and 450 °C, respectively (**Figure 2**). According to the DSC analysis, PαNDTDTNT did not show obvious melting point (T_m) below 350 °C, while PβNDTDTNT exhibited a T_m at 314 °C during heating and a crystallization point (T_c) at 292 °C during cooling (**Figure 3**), which implies that PαNDTDTNT is structurally more rigid than PβNDTDTNT.

2.2. UV–Vis Absorption Spectroscopy

The UV–vis absorption spectra of the polymers are shown in **Figure 4**. Both of the polymers showed two distinct bands in the absorption spectra. Compared to PβNDTDTNT showing the absorption maxima (λ_{max}) at 595 nm in *o*DCB solution (**Table 2** and Figure 4a), PαNDTDTNT exhibited broader absorption bands and a bathochromic shift of λ_{max} at 645 nm. The temperature-dependent absorption spectra were monitored at T = 25, 40, 60, 80, 100, 120, and 140 °C (**Figure 5**). As the temperature increases, the absorbance of two polymers was gradually hypsochromically shifted, suggesting that the strong polymeric interchain interactions occurring at room temperature are attenuated at high temperatures as a result of increased thermal motion around the polymer main chains. Therefore, the higher-temperature spectra can truly reflect the intrinsic optical transitions of a single polymer chain. The λ_{max} (580 nm) of PαNDTDTNT at 140 °C is more redshifted than that of

Table 1. Molecular weights and thermal properties of the polymers.

Polymer	M_n [kDa]	M_w [kDa]	PDI	T_d [°C]	T_g [°C]	T_m [°C]
PαNDTDTNT	67.3	86.4	1.3	446	122	
PβNDTDTNT	28.3	60.5	2.1	450		314

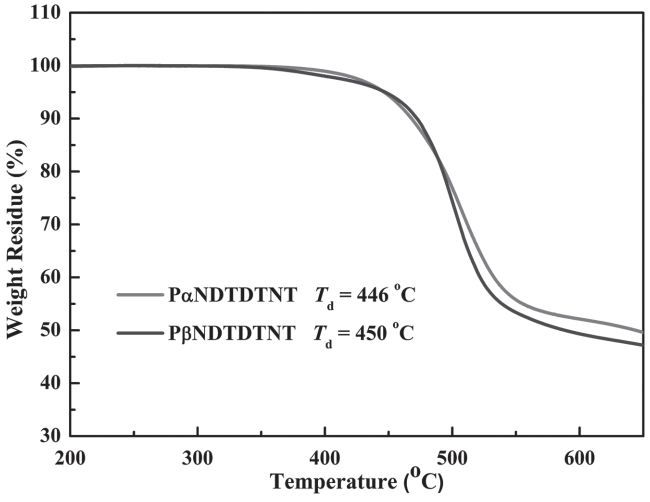

Figure 2. Thermogravimetric analysis of PαNDTDTNT and PβNDTDTNT at a ramping rate of 10 °C min^{-1}.

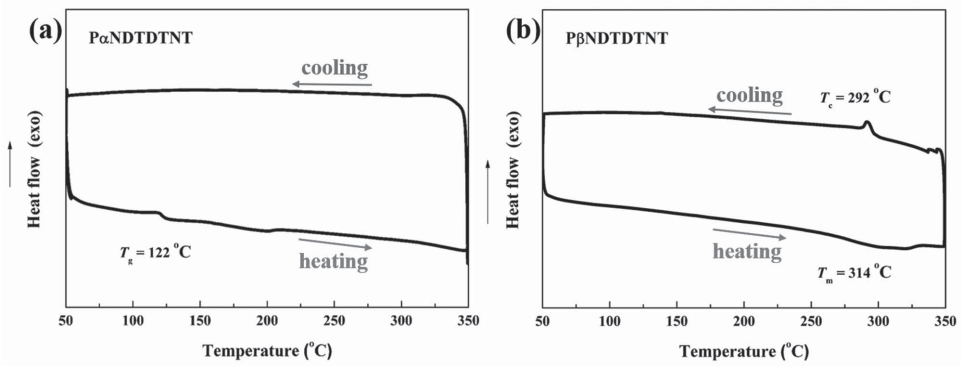

Figure 3. Differential scanning calorimetry of a) PαNDTDTNT and b) PβNDTDTNT at a ramping rate of 10 °C min^{-1}.

PβNDTDTNT (570 nm), suggesting that the αNDT segment induces more effective conjugation than the βNDT moiety. From 25 to 140 °C, λ_{max} of PαNDTDTNT and PβNDTDTNT is blueshifted by 65 and 25 nm, respectively, implying that PαNDTDTNT has stronger aggregation in solution.

In the thin film absorption spectra (Figure 4b), PαNDTDTNT exhibited a λ_{max} at 673 nm which is 60 nm bathochromic shift from that of PβNDTDTNT (613 nm). The optical band gaps (E_g^{opt}) calculated from the absorption onset of the solid state spectra were determined to be 1.58 eV for PαNDTDTNT (the onset at 786 nm) and 1.65 eV for PβNDTDTNT (the onset at 753 nm). Also note that PαNDTDTNT showed a pronounced vibronic shoulder in the longer wavelengths compared to PβNDTDTNT. The difference presumably results from the more linear polymer backbone of PαNDTDTNT to facilitate π-stacking in solid state, which will be discussed in the following sections. The broader absorption of PαNDTDTNT than that of PβNDTDTNT could be a beneficial factor for better photovoltaic properties.

2.3. Electrochemical Properties

Cyclic voltammetry (CV) was carried out to determine the highest ocuppied molecular orbital and lowest unocuppied molecular orbital (HOMO/LUMO) levels and the electrochemical band gaps of the polymers (Table 2 and **Figure 6**). The two polymers showed stable and reversible processes in the oxidative and reductive scans, which are important prerequisites for p-type organic semiconductors. The HOMO energy levels were estimated to be −5.40 eV for PαNDTDTNT and −5.46 eV for PβNDTDTNT. On the other hand, the LUMO energy levels are approximately located at −3.64 eV for PαNDTDTNT and −3.64 eV for PβNDTDTNT, which are higher than the LUMO level of the $PC_{71}BM$ (−3.8 eV) to ensure energetically favorable electron transfer. The Gaussian09 suite was applied to understand the molecular orbital properties of the polymeric π-electron systems. Two simplified trimer model compounds, denoted as TαNDTDTNT and TβNDTDTNT, are used for the calculations (**Figure 7**). All the aliphatic side chains are replaced by methyl groups. Quantum chemical calculations show that the HOMOs are homogeneously delocalized along the polymer chain, and the LUMOs are mostly localized on the NT acceptor region, which indicates evident intramolecular charge transfer between the donor and the acceptor upon excitation. The calculated HOMO and LUMO energy levels are −5.00 and −3.05 eV for TαNDTDTNT and −4.93 and −3.04 eV for TβNDTDTNT, respectively.

2.4. OFET Characteristics

The OFET mobilities of the polymers were measured by the devices using a bottom-gate/bottom-contact configuration with evaporated gold source/drain electrodes. The polymer films were spin-coated from the CB solutions, which

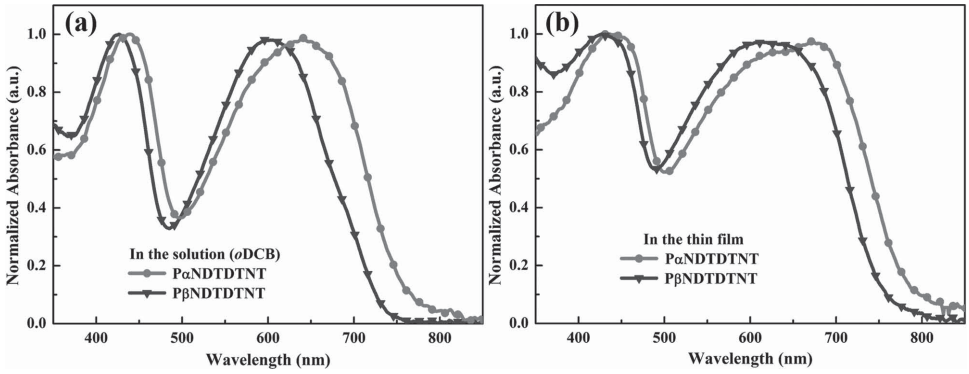

Figure 4. Normalized UV–vis absorption spectra of PαNDTDTNT, and PβNDTDTNT in a) *o*DCB solutions and b) the solid states.

Table 2. Optical and electrochemical properties.

Polymer	UV–vis λ_{max} [nm]		E_g^{opt} [eV]	E_{HOMO} [eV]	E_{LUMO} [eV]	E_g^{elect} [eV]
	*o*DCB at 25/140 °C	Film				
PαNDTDTNT	645/580	673	1.58	–5.40	–3.64	1.76
PβNDTDTNT	595/570	610	1.65	–5.46	–3.64	1.82

were subsequently annealed at 120 or 200 °C. The OFET devices used SiO_2 as gate dielectric whose surfaces were modified with octadecyltrichlorosilane (ODTS) to form a self-assembled monolayer (SAM). All of the output and transfer plots of the devices showed typical p-type OFET characteristics (**Figure 8**). The hole mobilities listed in **Table 3** with on/off ratios were calculated from the transfer characteristics of the devices in the saturation regime.

After annealed at 120 °C, PαNDTDTNT and PβNDTDTNT device exhibited similar hole mobilities of 0.019 $cm^2\ V^{-1}\ s^{-1}$ and 0.013 $cm^2\ V^{-1}\ s^{-1}$, respectively. However, with thermal annealing at 200 °C, the mobility of PβNDTDTNT is slightly improved to 0.038 $cm^2\ V^{-1}\ s^{-1}$, while PαNDTDTNT showed a substantial enhancement of the hole mobility reaching 0.214 $cm^2\ V^{-1}\ s^{-1}$ with an on–off ratio of 7.6×10^5. The high mobility of PαNDTDTNT is presumably due to the stronger π–π stacking of the polymer chains induced by the annealing process.

2.5. Polymer Ordering Structures in Solid State

In order to further understand the polymer ordering and the difference of the mobilities in the OFET devices between PαNDTDTNT and PβNDTDTNT, the ordering structures in the solid-state were investigated by 2D wide-angle X-ray diffraction (2D-WAXRD) studies. The polymers were annealed and sheared at 250 °C to form the polymer fibers. The 2D-WAXRD patterns were measured at room temperature with the X-ray incident beam perpendicular to the shearing direction which is along the meridian (**Figure 9**a,b). Both of the polymers exhibited diffraction arcs on the equator and meridian, suggesting the crystalline nature and the ordered phase of PαNDTDTNT and PβNDTDTNT. The diffractions of 1D-WAXRD at the equator as a function of 2θ are shown in Figure 9c. Both of the polymers exhibited (h00) peaks up to the third order at the small-angle region, indicating the highly ordered structures. PαNDTDTNT and PβNDTDTNT showed (100) peaks at 2θ of 3.80° and 3.88°, respectively, corresponding to d-spacings of 23.2 and 22.6 Å which are assigned to the backbone-to-backbone lamellar distances associated with the length of the lateral side chains. The similar distances of the conjugated polymer backbones are due to the fact that PαNDTDTNT and PβNDTDTNT possess the identical side chains that fill the periphery of the stacked backbone. On the other hand, at wide-angle region, PαNDTDTNT showed a pair of distinct diffraction arcs and a sharp (010) peak at 2θ of 25.0° which corresponds to the periodical π–π stacking distance ($d\pi$) of 3.56 Å between the facing conjugated backbones, whereas PβNDTDTNT exhibited halo-like diffractions and a corresponding broad (010) peak at 2θ of 22.6° with a $d\pi$ spacing of 3.93 Å. The π-stacking distance ($d\pi$) of 3.56 Å for PαNDTDTNT is relatively small compared to the other high-performance crystalline donor–acceptor copolymers. The more pronounced diffractions and closer $d\pi$ spacing support that PαNDTDTNT has a more ordered crystalline structure with stronger π–π stacking than PβNDTDTNT. These results are in good agreement with the stronger interchain aggregation of PαNDTDTNT observed in the UV–vis absorption spectra. Furthermore, considering that enhanced ordering structures generally facilitate the charge mobility, the structure analysis is also consistent with the trend of the OFET mobility for PαNDTDTNT and PβNDTDTNT.

2.6. Geometrical Effect of α-aNDT/β-aNDT Units on the Polymer Backbones

Both isomeric α-aNDT and β-aNDT are highly rigid and coplanar structures. Although PαNDTDTNT and PβNDTDTNT

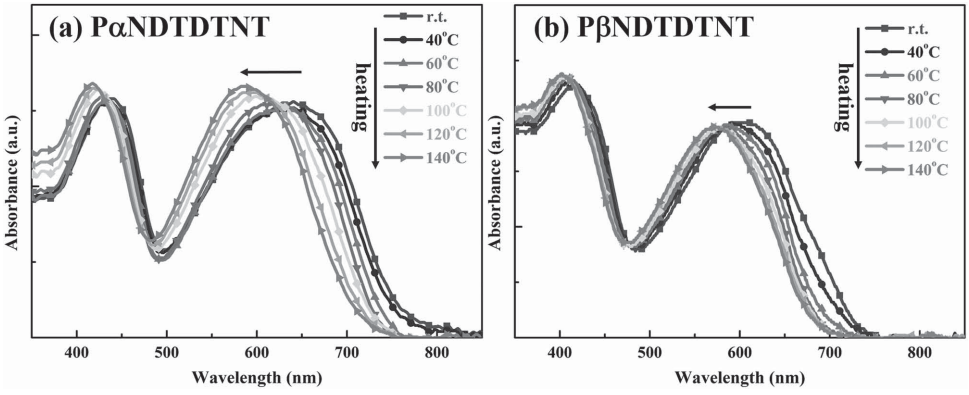

Figure 5. UV–vis absorption spectra of a) PαNDTDTNT and b) PβNDTDTNT in *o*DCB solutions at different temperatures.

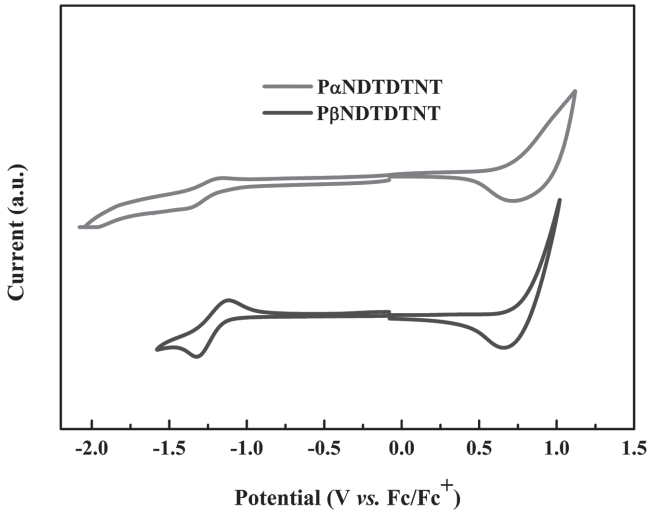

Figure 6. Cyclic voltammetry of PαNDTDTNT and PβNDTDTNT.

have similar structural compositions, it is obvious that the morphology of the two polymers in solid state is rather different. To further understand the nature of the distinct ordering structures in the isomeric α- and β-aNDT-based copolymers, we calculated the optimized backbone geometry of TαNDTDTNT and TβNDTDTNT model compounds as shown in **Figure 10**. Both TαNDTDTNT and TβNDTDTNT have sine-wave shapes but with different amplitudes. The angles between the horizontal axis of α-/β-aNDT donor units and that of NT units are used to quantify the difference in the backbone curvature. The angle was determined to be 148° for TαNDTDTNT and 126° for TβNDTDTNT. This analysis concludes that PαNDTDTNT possesses a more linear-shaped backbone than PβNDTDTNT, leading to better π–π stacking and more ordered packing structure in the thin film. Again, the result is in good agreement with the absorption spectra, OFET mobilities, and 2D-WAXRD analysis.

2.7. Quinoidal Structures of α-aNDT and β-aNDT in the Polymers

There are two mesomeric structures of a conjugated polymer including aromatic form and quinoidal form. The formation of quinoidal structures upon π-electron delocalization along the polymer chains would also play an important role in determining the polymer conformations. The quinoidal forms of α-aNDT[14] and β-aNDT segments denoted as q-αNDT and q-βNDT in the two isomeric polymers are illustrated in **Figure 11**. The geometry optimization of q-αNDT and q-βNDT moieties with two ethyl groups at 4,9-positions for simplicity was thus performed at the B3LYP/6-31G(d) level of theory. The results are summarized in **Figure 12**. The dihedral angles φ1(S)–2(C)–3(C)–4(C) and φ5(S)–6(C)–7(C)–8(C) between the two benzothiophene moieties in q-αNDT are very small (≈0.9°), indicating that the high coplanarity of αNDT moiety can be preserved from aromatic to quinoidal structures. However, the q-βNDT has much larger distortion with the dihedral angles φ1(S)–2(C)–3(C)–4(C) of –9.4° and φ5(S)–6(C)–7(C)–8(C) of –17.7°.

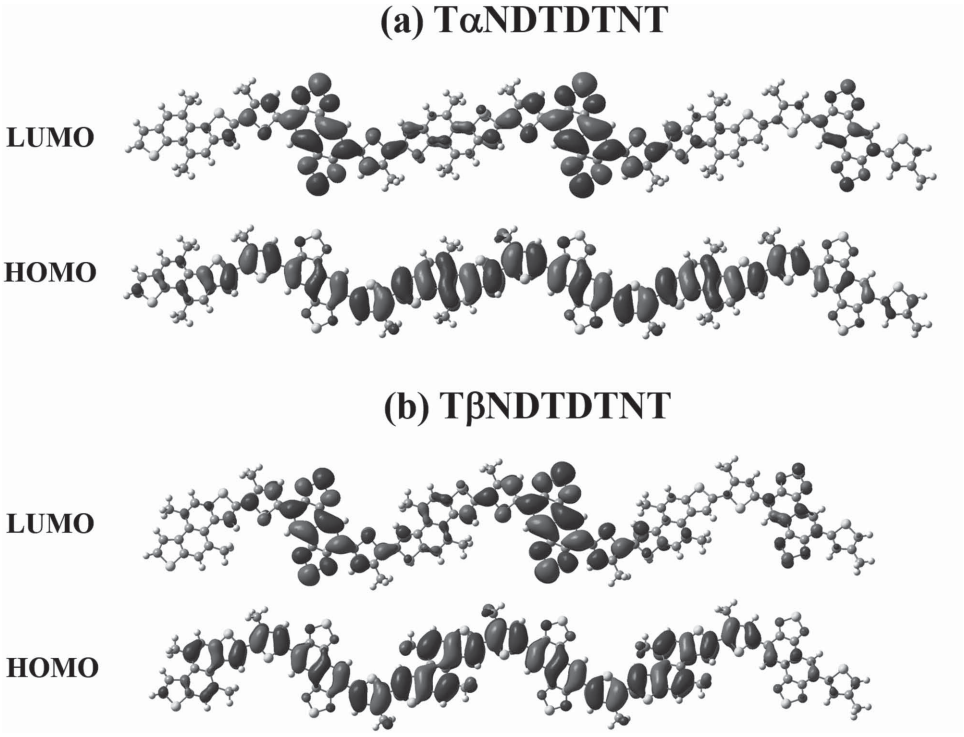

Figure 7. The HOMO and LUMO plots of the model compounds, a) TαNDTDTNT and b) TβNDTDTNT, calculated at the level of B3LYP/6-31G(d).

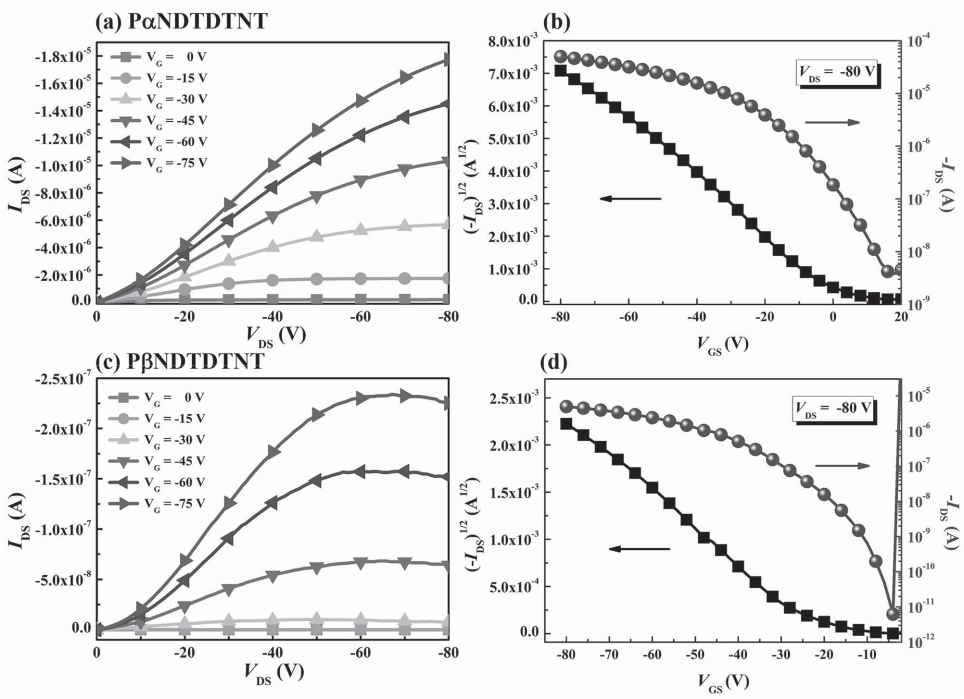

Figure 8. a,c) Typical output curves and b,d) transfer plots of the OFET devices based on PαNDTDTNT and PβNDTDTNT with the ODTS-SAM layer, respectively.

2.8. Coplanarity of α-aNDT and β-aNDT Moieties after Exciton Dissociation

The coplanarity of a natural polymer might change significantly after photoinduced electron transfer to generate a radical–cationic species. With the intention of further investigating the planarity of α-aNDT and β-aNDT units in the polymers after exciton dissociation, geometry optimization of two simplified structures, αNDTDT and βNDTDT, was calculated (the B3LYP/6-31G(d)) in both neutral and cationic states. The results are summarized in **Figure 13**. For αNDTDT, the dihedral angles φ1(S)–2(C)–3(C)–4(C) and φ5(S)–6(C)–7(C)–8(C) between the two benzothiophene moieties are close to 0° regardless of the neutral (Figure 13a) or cationic (Figure 13b) electronic states, indicating that the structural planarity of α-aNDT does not vary noticeably subsequent to the loss of one electron. With regard to β-aNDT system, the neutral βNDTDT already possesses slight distortion on the β-aNDT core (Figure 13c). The distortion is changed to a different manner when βNDTDT is situated in the radical–cationic state (Figure 13d). Overall, the computation results strongly suggest that α-aNDT moiety has more rigid and coplanar structure than β-aNDT, which might reduce reorganization energy for improving the charge mobility of PαNDTDTNT.[15]

Table 3. P-type OFET characteristics of the polymers.

Polymer	Annealing [°C]	V_{th} [V]	$I_{on/off}$	Mobility [cm^2 V^{-1} s^{-1}]
PαNDTDTNT	120	–0.54	3.24×10^4	0.019
	200	–0.89	7.60×10^5	0.214
PβNDTDTNT	120	–6.84	1.98×10^4	0.013
	200	–24.3	6.71×10^7	0.038

2.9. Photovoltaic Characteristics

The bulk heterojunction devices with an inverted architecture have better long-term stability than the conventional devices.[16] The inverted devices were thus fabricated based on the configuration of ITO/ZnO/PFN/polymer:$PC_{71}BM$/MoO_3/Ag, where the poly[(9,9-bis(3′-(*N*,*N*-dimethylamino)propyl)-2,7-fluorene)-alt-2,7-(9,9-dioctylfluorene)] (PFN)[17] is a buffer layer. The performance of conventional devices and inverted devices without using PFN is shown in Table S1 (Supporting Information). The current density–voltage characteristics and the external quantum efficiency (EQE) spectra of the devices under simulated 100 mW cm^{-2} AM 1.5 G illumination are shown in **Figure 14** and all the device parameters are shown in **Table 4**. The device using PαNDTDTNT:$PC_{71}BM$ (1:2, in wt%) delivered a PCE of 3.78% with a V_{oc} of 0.78, a moderate J_{sc} of 9.31, and a fill factor (FF) of 52%. By introducing 5 vol% diphenyl sulfide (DPS), the device efficiency further improved to 6.72% due to the increased V_{oc} of 0.84, FF of 58.4%, and J_{sc} of 13.70 mA cm^{-2}. To make a systematic comparison, the PβNDTDTNT:$PC_{71}BM$-based device using identical fabrication conditions (1:2 in wt% with 5 vol% DPS) showed a PCE of 3.6%, with a J_{sc} of 8.41 mA cm^{-2}, a V_{oc} of 0.80 V, and an FF of 53.5. The V_{oc} values of the PαNDTDTNT- and PβNDTDTNT-based devices are similar due to the small difference in their E_{HOMO} levels. Although PαNDTDTNT possesses lower extinction coefficient (Figure S1, Supporting Information), the device with PαNDTDTNT shows the much higher J_{sc} than that with PβNDTDTNT. It is likely

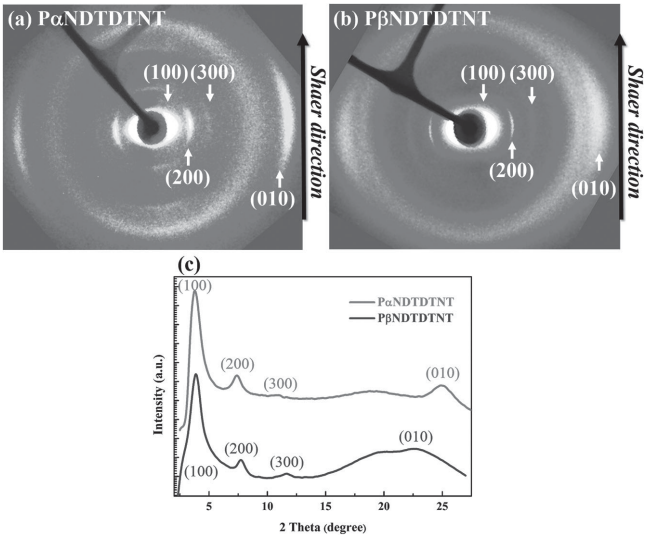

Figure 9. 2D-WAXD patterns of a) PαNDTDTNT and (b) PβNDTDTNT, c) 1D-WAXD diffractions at the equator.

attributed to the better film morphology of the active layer for the charge transportation leading to higher hole mobility of PαNDTDTNT. The grazing-incidence X-ray diffraction was thus employed to correlate the device performances with the morphology of the polymer/$PC_{71}BM$ blends (Figure S2, Supporting Information). The patterns of PαNDTDTNT/$PC_{71}BM$ blend showed a (200) peak and a sharp (100) peak at $2\theta = 3.8°$ with a d spacing (d_1) of 23.3 Å which corresponds to the lamellar structure along with side-chain interdigitation, whereas only negligible lamellar peak was observed for PβNDTDTNT/$PC_{71}BM$. The results again demonstrate that PαNDTDTNT is able to form a more ordered structure than PβNDTDTNT even when they are blended with $PC_{71}BM$, thereby producing higher J_{sc} in the PβNDTDTNT/$PC_{71}BM$-based device. We also conducted the space-charge-limited current (SCLC) mobility measurements for the two blend systems to evaluate vertical transport

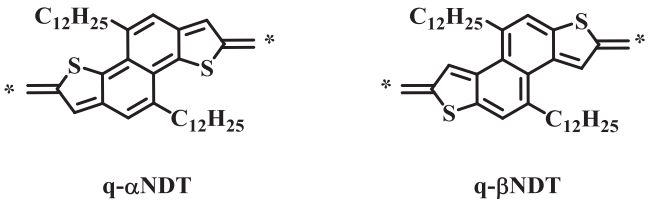

Figure 11. The quinoidal structures q-αNDT and q-βNDT in the polymers upon π–electron delocalization.

that ultimately determines the J_{sc} in the solar cells. The SCLC curves are included in Figure S3 (Supporting Information). The hole mobility of PαNDTDTNT:$PC_{71}BM$ blend (1:2.2 in wt%) is estimated to be 2.1×10^{-2} cm^2 V^{-1} s^{-1} which is an order of magnitude higher than that of PβNDTDTNT:$PC_{71}BM$ blend (1:2.2 in wt%) with 2.2×10^{-3} cm^2 V^{-1} s^{-1}.

To further optimize the device performance, the PαNDTDTNT:$PC_{71}BM$ device with 1:2.2 in wt% blend and 5 v% DPS delivered superior performance with a higher J_{sc} of 14.45 mA cm^{-2}, a V_{oc} of 0.78 V, an increased FF of 65.4%, and an improved PCE of 7.37%. By solvent annealing of the active layer for 30 min, a highest PCE of 8.01% with a V_{oc} of 0.80 V, an excellent J_{sc} of 15.55 mA cm^{-2}, and an FF of 64.4% was achieved. The corresponding EQEs for solar cells were measured under illumination of monochromatic light to check the accuracy of the measurements of the devices and the J_{sc} calculated from integration of the EQE spectra with an AM 1.5 G reference spectrum agrees well with the J_{sc} obtained from the J–V measurements.

2.10. Thin Film Morphology and AFM Images

Atomic force microscopy (AFM) was employed to examine the surface morphology of the blend films for better understanding the performance enhancement (**Figure 15**). Compared to the film without the additive (Figure 15a), the additive-processed PαNDTDTNT:$PC_{71}BM$ film (1:2, in wt%) with 5 vol% DPS

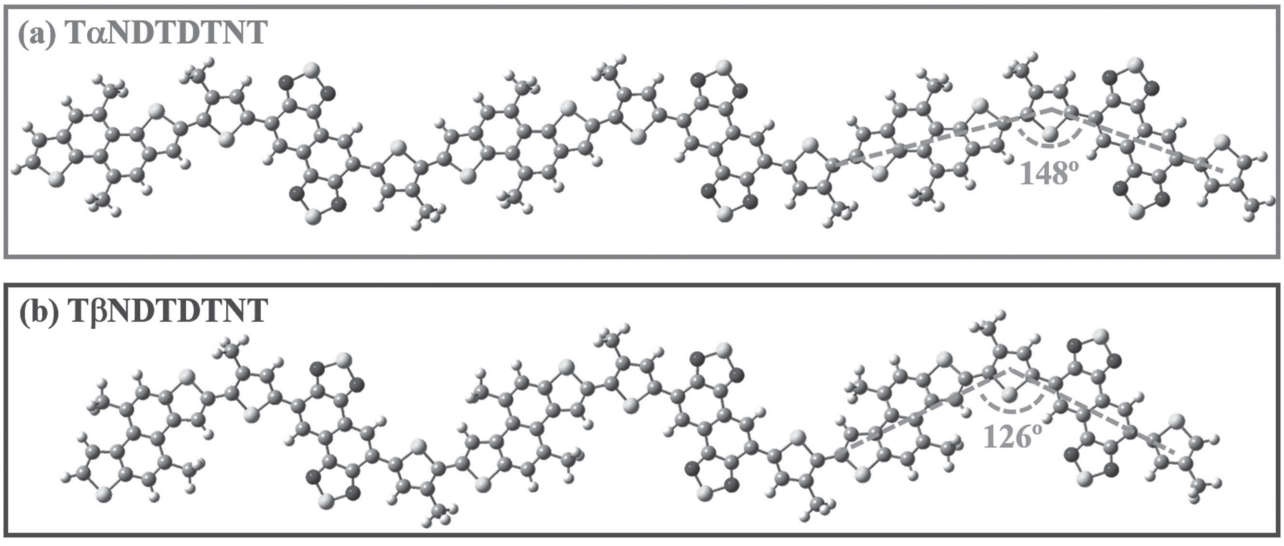

Figure 10. Optimized polymer backbone configurations of a) TαNDTDTNT and b) TβNDTDTNT.

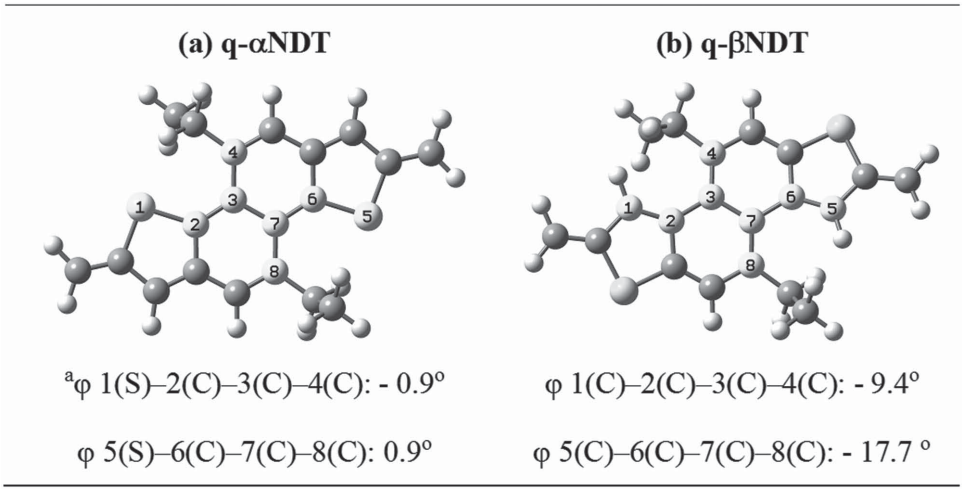

Figure 12. Optimized structures and dihedral angles between two benzothiophenes moieties of a) q-αNDT and b) q-βNDT. [a]φ = dihedral angle.

(Figure 15b) showed larger separation domains and greater surface roughness (5.52 vs 14.9 nm), suggesting that the DPS additive could influence the domains of the active layer to form the more favorable morphology leading to an increase of J_{sc} from 9.31 to 13.70 mA cm^{-2}. On the other hand, although the PαNDTDTNT:$PC_{71}BM$ blend (1:2.2 in wt%) with 5 vol% DPS film showed very similar surface roughness to that of the film treated with 30 min solvent annealing (Figure 15c,d), more pronounced fiber-like nanostructures were observed after solvent annealing, implying its more favorable morphological property for efficient charge separation and transporting properties to reach higher J_{sc} and PCE.

3. Conclusions

We have successfully developed two isomeric angular NDT building blocks, 4,9-dialkylated α-aNDT and β-aNDT,

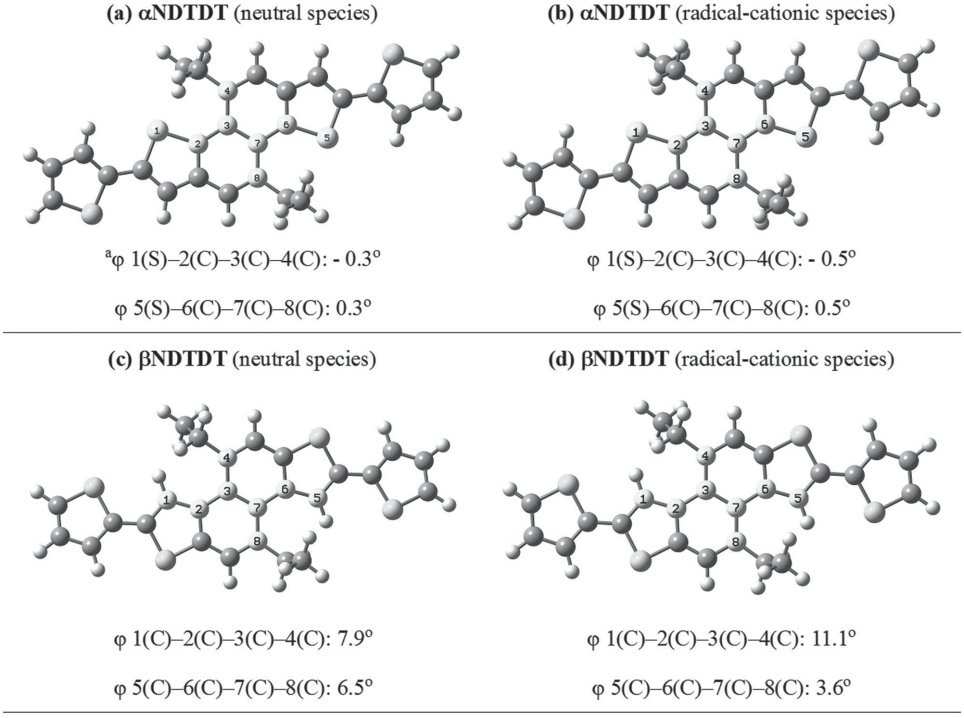

Figure 13. Optimized structures and dihedral angles between two benzothiophene moieties for a) αNDTDT (neutral species), b) αNDTDT (radical–cationic species), c) βNDTDT (neutral species), and d) βNDTDT (radical–cationic species). [a]φ = dihedral angle.

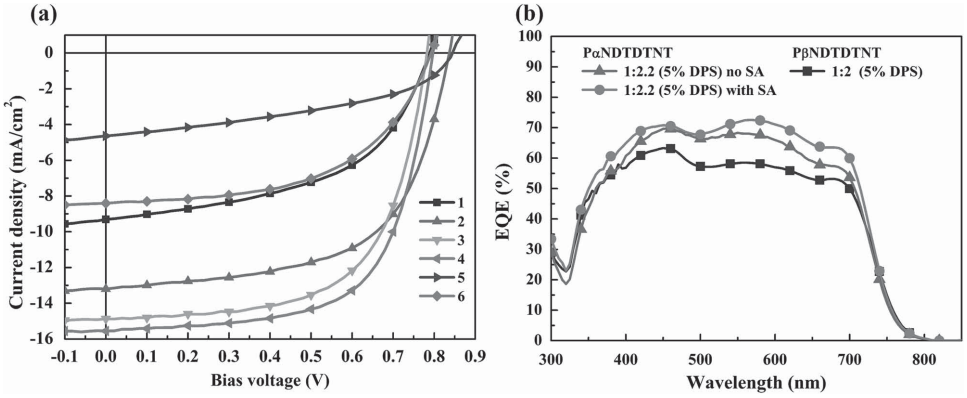

Figure 14. Current density–voltage characteristics of a) devices 1–6. b) EQE spectra of the devices under illumination of AM 1.5 G, 100 mW cm^{-2}.

synthesized by a regiospecific 6π-cyclization of the dithiophenyl-ene-diyne precursors. The distannylated α-aNDT and β-aNDT monomers are copolymerized to afford two isomeric donor–acceptor copolymers PαNDTDTNT and PβNDTDTNT. The molecular shape and geometry of the isomeric α-aNDT and β-aNDT subunits play a pivotal role in governing the conformation and packing of the resulting polymers. Theoretical calculations revealed that PαNDTDTNT has higher coplanarity and more linear polymer backbone than PβNDTDTNT. Consequently, PαNDTDTNT can assemble into more ordered π-stacking as well as lamellar stacking in the solid-state evidenced by the 2D-WAXD analysis. UV–vis spectroscopy also showed that PαNDTDTNT exhibited much more redshifted absorption than PβNDTDTNT both in solution and thin film because of the stronger intermolecular π–π interactions and better effective conjugation. Consistently, PαNDTDTNT exhibited a greater FET hole mobility of 0.214 cm^2 V^{-1} s^{-1} with an on–off ratio of 7.6 × 10^5, compared to PβNDTDTNT with a mobility of 0.038 cm^2 V^{-1} s^{-1} due to the higher ordering structure. More importantly, the solar cell devices based on the PαNDTDTNT:$PC_{71}BM$ blend delivered a superior efficiency of 8.01%.

4. Experimental Section

Materials: Unless otherwise stated, all reactions were carried out on a vacuum line under N_2 atmosphere. All chemicals were purchased from Sigma-Aldrich, TCI, Alfa Aesar, or Acros and used as received unless otherwise specified and all solvents were distilled before using. 3-bromothiophene-2-carbaldehyde (**1**), (*E*)-1,2-bis(3-bromothiophen-2-yl)ethene (**2**), 2-bromothiophene-3-carbaldehyde (**4**), and (*E*)-1,2-bis(2-bromothiophen-3-yl)ethane (**5**) were synthesized as reported.[12] Polymerization was operated with a microwave reactor, CEM Discover System. Polymer Average Molecular weights were determined by GPC with a Shodex KF-804 using THF as a solvent and calibrated with polystyrene standards.

*Synthesis of (E)-1,2-Bis(3-(tetradec-1-yn-1-yl)thiophen-2-yl)ethene (**3**)*: To a deoxygenated solution of compound **2** (1.50 g, 4.31 mmol) in THF (45 mL) and diisopropylamine (45 mL) was added $Pd(PPh_3)_2Cl_2$ (800 mg, 1.08 mmol, 25 mol%), CuI (196 mg, 1.08 mmol, 25 mol%), PPh_3 (282 mg, 1.08 mmol, 25 mol%) and tetradec-1-yne (2.10 g, 10.78 mmol). The mixture was stirred for 12 h at 80 °C, and water (60 mL) and hydrochloric acid (1 M, 60 mL) were then added. The resulting mixture was extracted with ethyl acetate (EA) (60 mL × 3), and the combined organic layer was dried over anhydrous $MgSO_4$, filtered, and concentrated in vacuo. The residue was purified by column chromatography on silica gel (hexane) to give a yellow solid **3** (yield: 95%). ^{1}H NMR ($CDCl_3$, 400 MHz): δ 7.31 (s, 2 H), 7.05 (d, J = 5.2 Hz, 2 H), 6.94 (d, J = 5.2 Hz, 2 H), 2.48 (t, J = 7.0 Hz, 4 H), 1.70–1.60 (m, 4 H), 1.56–1.55 (m, 4 H), 1.40–1.20 (m, 32 H), 0.88 (t, J = 6.8 Hz, 6 H); ^{13}C NMR ($CDCl_3$, 100 MHz): δ 143.85, 130.54, 123.07, 121.81, 121.17, 95.47, 75.07, 31.92, 29.69, 29.68, 29.65, 29.58, 29.56, 29.25, 28.98, 28.82, 22.68, 19.70, 14.11; MS (EI, $C_{38}H_{56}S_2$): calcd, 576.3823; found, 576.3823.

*Synthesis of (E)-1,2-Bis(2-(tetradec-1-yn-1-yl)thiophen-3-yl)ethene (**6**)*: In a similar manner to preparation of **3**, **6** was synthesized from compound **5** (1.00 g, 2.86 mmol) (yield: 97%). ^{1}H NMR ($CDCl_3$, 400 MHz): δ 7.24 (d, J = 5.4 Hz, 2 H), 7.18 (s, 2 H), 7.10 (d, J = 5.4 Hz, 2 H), 2.51 (t, J = 7.0 Hz, 4 H), 1.70–1.60 (m, 4 H), 1.50–1.40 (m, 4 H), 1.40–1.20 (m, 32 H), 0.88 (t, J = 7.0 Hz, 6 H); ^{13}C NMR ($CDCl_3$, 100 MHz): δ 142.12, 125.21,

Table 4. Photovoltaic properties of ITO/ZnO/PFN/polymer:$PC_{71}BM$/MoO_3/Ag-based solar cells.

Devices	Polymer	Polymer: $PCB_{71}M$ [w/w]	DPS [v/v,%]	V_{oc} [V]	J_{sc} [mA cm^{-2}]	FF [%]	PCE [%]
1	PαNDTDTNT	1:2	No	0.78	9.31	52.0	3.78
2	PαNDTDTNT	1:2	5	0.84	13.70	58.4	6.72
3	PαNDTDTNT	1:2.2	5	0.78	14.45	65.4	7.37
4	PαNDTDTNT	1:2.2	5[a)]	0.80	15.55	64.4	8.01
5	PβNDTDTNT	1:2	No	0.84	4.64	43.4	1.69
6	PβNDTDTNT	1:2	5	0.80	8.41	53.5	3.60

[a)]Solvent annealing for 30 min.

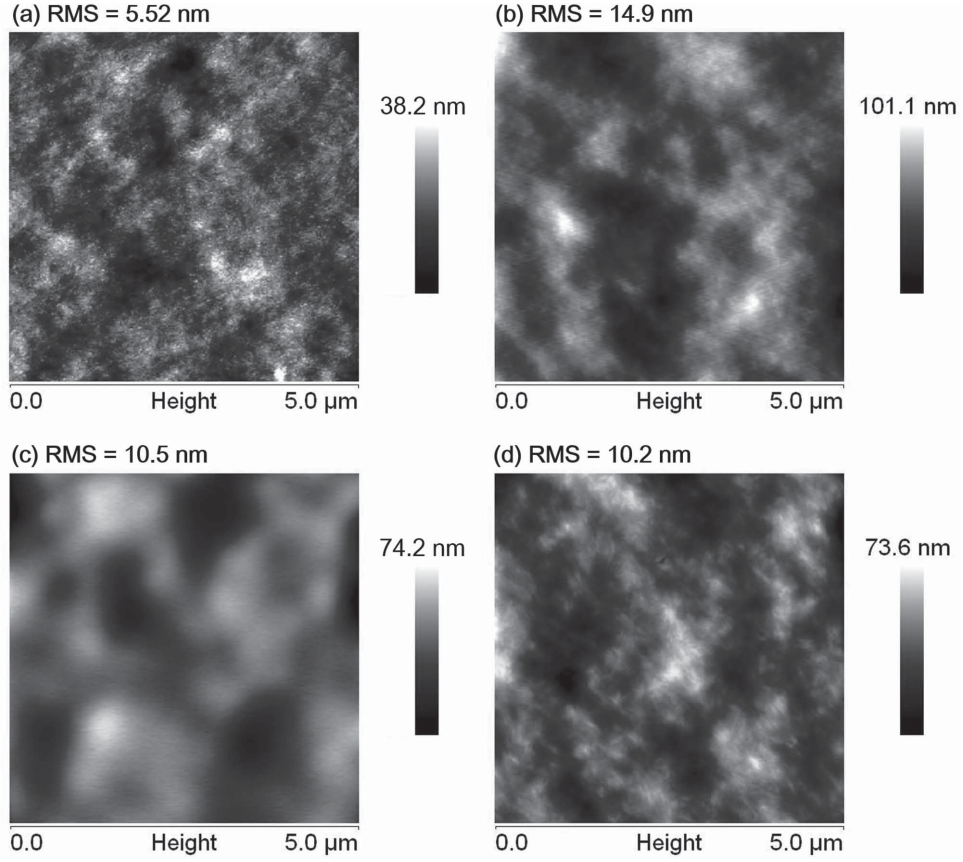

Figure 15. AFM height images (5.0 μm × 5.0 μm) of the surface of PαNDTDTNT:$PC_{71}BM$ blends a) 1:2 without DPS additives, b) 1:2 with 5 vol% DPS, c) 1:2.2 with 5 vol% DPS before solvent annealing, and d) 1:2.2 with 5 vol% DPS after 30 min solvent annealing.

124.00, 122.63, 121.07, 99.24, 73.11, 31.90, 29.66, 29.65, 29.62, 29.57, 29.34, 29.20, 29.00, 28.68, 22.67, 19.97, 14.10; MS (EI, $C_{38}H_{56}S_2$): calcd, 576.3823; found, 576.3822.

Synthesis of 4,9-Didodecylnaphtho[1,2-b:5,6-b′]dithiophene (α-aNDT): To a deoxygenated *N*-methyl-2-pyrrolidone (10 mL) solution of compound **3** (1.94 g, 3.36 mmol) was added DBU (0.95 mL, 6.72 mmol). The resulting mixture was refluxed for 2 d, cooled to room temperature (RT), diluted with water (100 mL), and extracted with EA (15 mL × 3). The combined organic layer was washed with brine solution (15 mL) and dried over anhydrous $MgSO_4$. After filtration, the solvent was removed under vacuum and the residue was purified by column chromatography on silica gel (hexane) to give a white solid α-aNDT (yield: 70%). ^{1}H NMR ($CDCl_3$, 400 MHz): δ 7.91 (s, 2 H), 7.59 (d, J = 5.6 Hz, 2 H), 7.49 (d, J = 5.6 Hz, 2 H), 3.52 (t, J = 8.0 Hz, 4 H), 1.95–1.80 (m, 4 H), 1.65–1.58 (m, 4 H), 1.50–1.20 (m, 32 H), 0.89 (t, J = 6.8 Hz, 6 H); ^{13}C NMR ($CDCl_3$, 100 MHz): δ 137.59, 135.91, 134.25, 128.17, 125.85, 123.71, 123.60, 37.02, 31.93, 31.23, 29.82, 29.70, 29.68, 29.66, 29.36, 22.69, 14.12; MS (EI, $C_{38}H_{56}S_2$): calcd, 576.3823; found, 576.3827.

Synthesis of 4,9-Didodecylnaphtho[2,1-b:6,5-b′]dithiophene (β-aNDT): In a similar manner to preparation of *α-aNDT*, *β-aNDT* was synthesized from **6** (2.0 g, 3.47 mmol) (yield: 82%). ^{1}H NMR ($CDCl_3$, 400 MHz): 8.15 (d, J = 5.6 Hz, 2 H), δ 7.94 (s, 2 H), 7.54 (d, J = 5.6 Hz, 2 H), 3.43 (t, J = 8.0 Hz, 4 H), 1.90–1.80 (m, 4 H), 1.60–1.50 (m, 4 H), 1.40–1.20 (m, 32 H), 0.88 (t, J = 6.8 Hz, 6 H); ^{13}C NMR ($CDCl_3$, 100 MHz): δ 138.64, 136.20, 133.66, 128.37, 126.63, 123.48, 122.71, 38.27, 31.91, 30.80, 29.81, 29.67, 29.65, 29.64, 29.63, 29.59, 29.34, 22.68, 14.11; MS (EI, $C_{38}H_{56}S_2$) calcd, 576.3823; found, 576.3822.

Synthesis of 2,7-Bis(trimethylstannyl)-4,9-didodecylnaphtho[1,2-b:5,6-b′]dithiophene (Sn-α-aNDT): To an anhydrous THF (20 mL) solution of α-aNDT (500 mg, 0.867 mmol) was added *n*-butyllithium (0.76 mL, 2.5 M) slowly at –78 °C. The stirring was continued for 30 min at –78 °C and subsequently for 30 min at RT. After cooling to –78 °C, trimethyltin chloride (2.17 mL, 1 M) was added in one portion. The mixture was slowly warmed to RT and stirred for 6 h. It was quenched with saturated NH_4Cl solution (10 mL). The organic layer was separated and the aqueous layer was extracted with EA (10 mL). The combined organic extract was washed with brine solution (20 mL × 3) and dried over anhydrous $MgSO_4$. After filtration, the solvent was removed under vacuum to give a white solid Sn-α-aNDT (yield: 88%). ^{1}H NMR ($CDCl_3$, 400 MHz): δ 7.90 (s, 2 H), 7.57 (s, 2 H), 3.55 (t, J = 8.0 Hz, 4 H), 1.90–1.80 (m, 4 H), 1.70–1.58 (m, 4 H), 1.50–1.20 (m, 32 H), 0.89 (t, J = 6.8 Hz, 6 H), 0.49 (s, 18 H); ^{13}C NMR ($CDCl_3$, 100 MHz): δ 139.43, 138.84, 138.82, 136.06, 131.78, 127.62, 122.87, 37.06, 31.94, 31.28, 29.81, 29.72, 29.71, 29.68, 29.67, 29.37, 22.69, 14.12, –8.24; MS (APCI, $C_{44}H_{72}S_2Sn_2$): calcd, 904.3114; found, 904.3145.

Synthesis of 2,7-Bis(trimethylstannyl)-4,9-didodecylnaphtho[2,1-b:6,5-b′]dithiophene (Sn-β-aNDT): In a similar manner to preparation of *Sn-α-aNDT*, *Sn-β-aNDT* was synthesized from *β-aNDT* (1.0 g, 1.73 mmol) (yield: 85%). ^{1}H NMR ($CDCl_3$, 400 MHz): δ 8.18 (s, 2 H), 7.95 (s, 2 H), 3.44 (t, J = 8.0 Hz, 4 H), 1.90–1.80 (m, 4 H), 1.60–1.50 (m, 4 H), 1.40–1.10 (m, 32 H), 0.89 (t, J = 6.8 Hz, 6 H), 0.48 (s, 18 H); ^{13}C NMR ($CDCl_3$, 100 MHz): δ 143.23, 136.49, 135.69, 135.20, 134.30, 127.87, 122.38, 38.69, 31.92, 31.30, 30.14, 29.76, 29.71, 29.68, 29.64, 29.35, 22.69, 14.12, –8.25; MS (APCI, $C_{44}H_{72}S_2Sn_2$) calcd, 904.3114; found, 904.3131.

Synthesis of PαNDTDTNT: To a 50 mL round-bottom flask was introduced Sn-α-aNDT (84 mg, 0.093 mmol), Br-DTNT-HD (94 mg, 0.093 mmol), tris(dibenzylideneacetone)dipalladium (3.40 mg, 0.0037 mmol), tri(2-methylphenyl)phosphine (9.1 mg, 0.03 mmol), and deoxygenated CB (4 mL). The mixture was then degassed by bubbling nitrogen for 10 min at room temperature. The round-bottom flask was placed into

the microwave reactor and refluxed for 50 min under 270 W. Then, tributyl(thiophen-2-yl)stannane (17.3 mg, 0.046 mmol) was added to the mixture solution and reacted for 10 min under 270 W. Finally, 2-bromothiophene (8.2 mg, 0.050 mmol) was added to the mixture solution and reacted for 10 min under 270 W. The solution was added into methanol dropwise. The precipitate was collected by filtration and washed by Soxhlet extraction with acetone (24 h) and hexane (24 h) sequentially. The product was redissolved in hot CB (200 mL). The Pd-thiol gel (Silicycle Inc.) was added to the above CB solution to remove the residual Pd catalyst at 80 °C for 1 h. After filtration of solution and removal of the solvent under reduced pressure, the polymer solution was added into methanol to reprecipitate. The purified polymer was collected by filtration and dried under vacuum for 1 d to give a purple black solid (110 mg, yield 82%).

Synthesis of PβNDTDTNT: To a 50 mL round-bottom flask was introduced Sn-β-aNDT (88.9 mg, 0.0985 mmol), Br-DTNT-HD (100.0 mg, 0.0985 mmol), tris(dibenzylideneacetone)dipalladium (3.61 mg, 0.00394 mmol), tri(2-methylphenyl)phosphine (9.6 mg, 0.0315 mmol), and deoxygenated CB (4.0 mL). The mixture was then degassed by bubbling nitrogen for 10 min at room temperature. The round-bottom flask was placed into the microwave reactor and refluxed for 50 min under 270 W. Then, tributyl(thiophen-2-yl)stannane (18.38 mg, 0.0493 mmol) was added to the mixture solution and reacted for 10 min under 270 W. Finally, 2-bromothiophene (8.67 mg, 0.0532 mmol) was added to the mixture solution and reacted for 10 min under 270 W. The solution was added into methanol dropwise. The precipitate was collected by filtration and washed by Soxhlet extraction with acetone (24 h) and hexane (24 h) sequentially. The product was redissolved in hot CB (200 mL). The Pd-thiol gel (Silicycle Inc.) was added to the above CB solution to remove the residual Pd catalyst at 80 °C for 1 h. After filtration of solution and removal of the solvent under reduced pressure, the polymer solution was added into methanol to reprecipitate. The purified polymer was collected by filtration and dried under vacuum for 1 d to give a purple black solid (100 mg, yield 71%). ^{1}H NMR ($CDCl_3$, 400 MHz): δ 8.80–8.00 (br, 4 H), 7.90–7.30 (br, 4 H), 3.60–2.60 (br, 8 H), 2.10–0.40 (br, 108 H).

General Measurement and Characterization: ^{1}H and ^{13}C NMR spectra were measured using a Varian 400 MHz instrument spectrometer and obtained in deuterated chloroform ($CDCl_3$) with tetramethylsilane (TMS) as internal reference unless otherwise stated, and chemical shifts (δ) are reported in parts per million. TGA was recorded on a Perkin Elmer Pyris under nitrogen atmosphere at a heating rate of 10 °C min^{-1}. DSC was measured on a TA Q200 Instrument under nitrogen atmosphere at a heating rate of 10 °C min^{-1}. Absorption spectra were taken on an HP8453 UV–vis spectrophotometer. Electrochemical CV was conducted on a CH instruments electrochemical analyzer. A carbon glass was used as the working electrode, Pt wire was used as the counter electrode, and Ag/Ag$^+$ electrode (0.01 M $AgNO_3$, 0.1 M TBAP in acetonitrile) was used as the reference electrode in a solution of dichloromethane with 0.1 M $TBAPF_6$ (tetrabutylammonium hexafluorophosphate) at 80 mV s^{-1}. CV curves were calibrated using ferrocene as the standard, and the $E_{1/2}$ of ferrocene is 0.09 V calculated as the average of the two peak maxima E_{pa} and E_{pc}. The HOMO energy levels were obtained from the equation HOMO = $-(E_{ox}^{onset} - E_{1/2(ferrocene)} + 4.8)$ eV and the LUMO energy levels were obtained from the equation LUMO = $-(E_{red}^{onset} - E_{1/2(ferrocene)} + 4.8)$ eV. For 2D-WAXD patterns, Bruker APEX DUO single crystal diffraction was applied and an INCOATEC 18 kW rotating I microfocus X-ray generator (Cu-Kα radiation (λ = 0.1542 nm)) attached to an APEX II CCD camera was used. The exposure time to obtain high-quality patterns was 40 s. Quantum chemical calculations were performed with the Gaussian09 suite employing the B3LYP density functional in combination with the 6-31G(d) basis set. Geometry optimizations were performed by applying tight self-consistent field (SCF) and convergence criteria and an ultrafine integration grid by applying the a geometry optimization method using an energy-represented direct inversion in the iterative subspace algorithm (GEDIIS) optimization algorithm. The minimum nature of each stationary point was confirmed by a frequency analysis.

OFET Device Fabrication and Characterization: Bottom-gate, bottom-contact OFETs were fabricated on Si/SiO_2 substrates with Ti/Au electrodes. An n-type heavily doped Si wafer with an SiO2 layer of 300 nm and a capacitance of 11 nF cm^{-2} was used as the gate electrode and dielectric layer. Gold source and drain contacts (40 nm in thickness) were deposited by vacuum evaporation after titanium on ODTS-treated SiO_2/Si substrates through the same shadow mask. The gold source and drain contacts were treated with the pentafluorothiophenol SAM. The channel width and length of the transistors are 1.00 and 0.100 mm, respectively. The polymers were dissolved in CB (10 mg mL^{-1}) and spin-coated at 1000 rpm from a hot solution before being annealed at 200 °C for 10 min. Electrical measurements of OTFT devices were carried out at room temperature in vacuum using a 4156C, Agilent Technologies. The field-effect mobility was calculated in the saturation regime by using the equation $I_{ds} = (\mu W C_i/2L)(V_g - V_t)^2$, where I_{ds} is the drain–source current, μ is the field-effect mobility, W is the channel width, L is the channel length, C_i is the capacitance per unit area of the gate dielectric layer, V_g is the gate voltage, and V_t is the threshold voltage.

OPV Device Fabrication and Characterization: Indium tin oxide (ITO)/glass substrates were ultrasonically cleaned sequentially in detergent, water, acetone, and isopropyl alcohol. Then, the ZnO precursor solution was spin-coated onto ITO-coated glass and followed by thermal annealing at 170 °C in air for 15 min to crystallize the film (thickness ≈50 nm). Subsequently, the PFN interlayer material was dissolved in methanol in the presence of a small amount of acetic acid (2 μL mL^{-1}) and its solution (concentration, 2 mg mL^{-1}) was spin-coated on top of the ZnO layer. Polymers were dissolved in *o*-dichlorobenzene (ODCB) and $PC_{71}BM$ (purchased from UR) was added to reach the desired ratio. The solution was stirred at 80 °C overnight and then heated at 110 °C for 1 h before spin-coating. The photoactive layers were then spin-coated in a glovebox. The polymer/ODCB concentration is 10 mg mL^{-1} and the spin-coating speed is 600 rpm. An MoO_3 layer (thickness = ≈7 nm) and silver top anode (thickness = ≈150 nm) were then thermally evaporated through a shadow mask under high vacuum (<1×10^{-6} Torr) to complete the inverted devices. Each device is constituted of four pixels defined by an active area of 0.04 cm^2. Finally, the *J–V* curves were measured in air under AM 1.5 G spectrum from a solar simulator.

Supporting Information

Supporting Information is available from the Wiley Online Library or from the author.

Acknowledgements

The authors thank the Ministry of Science and Technology, the Ministry of Education, and the Center for Interdisciplinary Science (CIS) of the National Chiao Tung University, Taiwan, for financial support and the National Center of High-Performance Computing (NCHC) in Taiwan for computer time and facilities. They also thank Prof. Chien-Lung Wang at NCTU for help with the 2D-WAXRD measurements. Y.J.C. acknowledges support from the Golden–Jade fellowship of the Kenda Foundation, Taiwan. This work was partially supported by Grants-in-Aid for Scientific Research (24685030 and 15H02196) from Japan Society for the Promotion of Science.

Received: June 9, 2015
Revised: July 10, 2015
Published online: September 14, 2015

[1] a) J.-S. Wu, S.-W. Cheng, Y.-J. Cheng, C.-S. Hsu, *Chem. Soc. Rev.* **2015**, *44*, 1113; b) Y. Li, *Acc. Chem. Res.* **2012**, *45*, 723; c) X. Zhao, X. Zhan, *Chem. Soc. Rev.* **2011**, *40*, 3728; d) Y.-J. Cheng, S.-H. Yang, C.-S. Hsu, *Chem. Rev.* **2009**, *109*, 5868; e) C. H. Duan, F. Huang, Y. Cao, *J. Mater. Chem.* **2012**, *22*, 10416; f) H. Zhou, L. Yang, W. You, *Macromolecules* **2012**, *45*, 607; g) J. W. Chen, Y. Cao, *Acc. Chem. Res.* **2009**, *42*, 1709; h) Y. F. Li, Y. P. Zou, *Adv. Mater.* **2008**, *20*, 2952; i) H. J. Son, B. Carsten, I. H. Jung, L. Yu, *Energy Environ. Sci.* **2012**, *5*, 8158.

[2] a) M. Leclerc, J.-F. Morin, *Design and Synthesis of Conjugated Polymers*, Wiley-VCH Verlag GmbH & Co. KGaA, Weinheim, Germany **2010**; b) T. A. Skotheim, J. Reynolds, *Handbook of Conducting Polymers*, 3rd ed., CRC Press, Boca Raton, FL, USA **2007**; c) H. Sirringhaus, P. J. Brown, R. H. Friend, M. M. Nielsen, K. Bechgaard, B. M. W. Langeveld-Voss, A. J. H. Spiering, R. A. J. Janssen, E. W. Meijer, P. Herwig, D. M. De Leeuw, *Nature* **1999**, *401*, 685; d) I. McCulloch, M. Heeney, C. Bailey, K. Genevicius, I. MacDonald, M. Shkunov, D. Sparrowe, S. Tierney, R. Wagner, W. Zhang, M. L. Chabinyc, R. J. Kline, M. D. McGehee, M. F. Toney, *Nat. Mater.* **2006**, *5*, 328; e) I. McCulloch, M. Heeney, M. L. Chabinyc, D. DeLongchamp, R. J. Kline, M. Cölle, W. Duffy, D. Fischer, D. Gundlach, B. Hamadani, R. Hamilton, L. Richter, A. Salleo, M. Shkunov, D. Sparrowe, S. Tierney, W. Zhang, *Adv. Mater.* **2009**, *21*, 1091; f) M. L. Chabinyc, M. F. Toney, R. J. Kline, I. McCulloch, M. Heeney, *J. Am. Chem. Soc.* **2007**, *129*, 3226; g) I. Osaka, R. D. McCullough, *Acc. Chem. Res.* **2008**, *41*, 1202; h) B. S. Ong, Y. Wu, P. Liu, S. Gardner, *J. Am. Chem. Soc.* **2004**, *126*, 3378.

[3] R. Rieger, D. Beckmann, A. Mavrinskiy, M. Kastler, K. Müllen, *Chem. Mater.* **2010**, *22*, 5314.

[4] a) G. Zuo, Z. Li, M. Zhang, X. Guo, Y. Wu, S. Zhang, B. Peng, W. Wei, J. Hou, *Polym. Chem.* **2014**, *5*, 1976; b) Y. Wu, Z. Li, W. Ma, Y. Huang, L. Huo, X. Guo, M. Zhang, H. Ade, J. Hou, *Adv. Mater.* **2013**, *25*, 3449.

[5] a) T. Lei, J.-Y. Wang, J. Pei, *Acc. Chem. Res.* **2014**, *47*, 1117; b) T. Lei, Y. Cao, X. Zhou, Y. Peng, J. Bian, J. Pei, *Chem. Mater.* **2012**, *24*, 1762.

[6] a) I. Osaka, Y. Houchin, M. Yamashita, T. Kakara, N. Takemura, T. Koganezawa, K. Takimiya, *Macromolecules* **2014**, *47*, 3502; b) K. R. Graham, C. Cabanetos, J. P. Jahnke, M. N. Idso, A. E. Labban, G. O. N. Ndjawa, T. Heumueller, K. Vandewal, A. Salleo, B. F. Chmelka, A. Amassian, P. M. Beaujuge, M. D. McGehee, *J. Am. Chem. Soc.* **2014**, *136*, 9608; c) J. Li, X. Qiao, Y. Xiong, H. Li, D. Zhu, *Chem. Mater.* **2014**, *26*, 5782; d) J. Mei, Z. Bao, *Chem. Mater.* **2014**, *26*, 604; e) H.-H. Chang, C.-E. Tsai, Y.-Y. Lai, W.-W. Liang, S.-L. Hsu, C.-S. Hsu, Y.-J. Cheng, *Macromolecules* **2013**, *46*, 7715; f) R. J. Kline, D. M. DeLongchamp, D. A. Fischer, E. K. Lin, L. J. Richter, M. L. Chabiny, M. F. Toney, M. Heeney, I. McCulloch, *Macromolecules* **2007**, *40*, 7960.

[7] a) H.-Y. Chen, J. Hou, S. Zhang, Y. Liang, G. Yang, Y. Yang, L. Yu, Y. Wu, G. Li, *Nat. Photonics* **2009**, *3*, 649; b) L. Huo, S. Zhang, X. Guo, F. Xu, Y. Li, J. Hou, *Angew. Chem. Int. Ed.* **2011**, *50*, 9697; c) L. Huo, J. Hou, *Polym. Chem.* **2011**, *2*, 2453; d) H. J. Son, W. Wang, T. Xu, Y. Liang, Y. Wu, G. Li, L. Yu, *J. Am. Chem. Soc.* **2011**, *133*, 1885; e) Y.-L. Chen, C.-Y. Chang, Y.-J. Cheng, C.-S. Hsu, *Chem. Mater.* **2012**, *24*, 3964; f) L. Ye, S. Zhang, L. Huo, M. Zhang, J. Hou, *Acc. Chem. Res.* **2014**, *47*, 1595; g) M. Zhang, X. Guo, S. Zhang, J. Hou, *Adv. Mater.* **2014**, *26*, 1118; h) M. Zhang, X. Guo, W. Ma, S. Zhang, L. Huo, H. Ade, J. Hou, *Adv. Mater.* **2014**, *26*, 2089; i) L. Lu, L. Yu, *Adv. Mater.* **2014**, *26*, 4413; j) L. Ye, S. Zhang, W. Zhao, H. Yao, J. Hou, *Chem. Mater.* **2014**, *26*, 3603.

[8] a) K. Takimiya, I. Osaka, *Chem. Rec.* **2015**, *15*, 175; b) X. Zhu, J. Fang, K. Lu, J. Zhang, L. Zhu, Y. Zhao, Z. Shuai, Z. Wei, *Chem. Mater.* **2014**, *26*, 6947; c) I. Osaka, T. Kakara, N. Takemura, T. Koganezawa, K. Takimiya, *J. Am. Chem. Soc.* **2013**, *135*, 8834; d) S. Shi, P. Jiang, S. Yu, L. Wang, X. Wang, M. Wang, H. Wang, Y. Li, X. Li, *J. Mater. Chem. A* **2013**, *1*, 1540; e) S. Shi, X. Xie, P. Jiang, S. Chen, L. Wang, M. Wang, H. Wang, X. Li, G. Yu, Y. Li, *Macromolecules* **2013**, *46*, 3358; f) C. Bathula, C. E. Song, S. Badgujar, S.-J. Hong, S. Y. Park, W. S. Shin, J.-C. Lee, S. Cho, T. Ahn, S.-J. Moon, S. K. Lee, *Polym. Chem.* **2013**, *4*, 2132; g) I. Osaka, T. Abe, M. Shimawaki, T. Koganezawa, K. Takimiya, *ACS Macro Lett.* **2012**, *1*, 437; h) S. R. Sanjaykumar, S. Badgujar, C. E. Song, W. S. Shin, S.-J. Moon, I.-N. Kang, J. Lee, S. Cho, S. K. Lee, J.-C. Lee, *Macromolecules* **2012**, *45*, 6938; i) I. Osaka, T. Abe, S. Shinamura, E. Miyazaki, K. Takimiya, *J. Am. Chem. Soc.* **2010**, *132*, 5000; j) S. Shinamura, E. Miyazaki, K. Takimiya, *J. Org. Chem.* **2010**, *75*, 1228.

[9] a) M. Nakano, H. Mori, S. Shinamura, K. Takimiya, *Chem. Mater.* **2012**, *24*, 190; b) Q. Peng, Q. Huang, X. Hou, P. Chang, J. Xu, S. Deng, *Chem. Commun.* **2012**, *48*, 11452; c) S. Loser, H. Miyauchi, J. W. Hennek, J. Smith, C. Huang, A. Facchetti, T. J. Marks, *Chem. Commun.* **2012**, *48*, 8511; d) S. Loser, C. J. Bruns, H. Miyauchi, R. P. Ortiz, A. Facchetti, S. I. Stupp, T. J. Marks, *J. Am. Chem. Soc.* **2011**, *133*, 8142; e) S. R. Sanjaykumar, S. Badgujar, C. E. Song, W. S. Shin, S.-J. Moon, I.-N. Kang, J. Lee, S. Cho, S. K. Lee, J.-C. Lee, *Macromolecules* **2012**, *45*, 6938; f) R. S. Koti, S. R. Sanjaykumar, S.-J. Hong, C. E. Song, I.-N. Kang, S. K. Lee, W. S. Shin, S.-J. Moon, J.-C. Lee, *Sol. Energy Mater. Sol. Cells* **2013**, *108*, 213.

[10] a) I. Osaka, K. Komatsu, T. Koganezawa, K. Takimiya, *Sci. Technol. Adv. Mater.* **2014**, *15*, 024201; b) I. Osaka, S. Shinamura, T. Abea, K. Takimiya, *J. Mater. Chem. C* **2013**, *1*, 1297; c) M. Nakano, S. Shinamura, Y. Houchin, I. Osaka, E. Miyazaki, K. Takimiya, *Chem. Commun.* **2012**, *48*, 5671; d) I. Osaka, T. Abe, S. Shinamura, K. Takimiya, *J. Am. Chem. Soc.* **2011**, *133*, 6852; e) S. Shinamura, I. Osaka, E. Miyazaki, A. Nakao, M. Yamagishi, J. Takeya, K. Takimiya, *J. Am. Chem. Soc.* **2011**, *133*, 5024.

[11] a) S. Shinamura, R. Sugimoto, N. Yanai, N. Takemura, T. Kashiki, I. Osaka, E. Miyazaki, K. Takimiya, *Org. Lett.* **2012**, *14*, 4718; b) M. Nakano, S. Shinamura, R. Sugimoto, I. Osaka, E. Miyazaki, K. Takimiya, *Org. Lett.* **2012**, *14*, 5448.

[12] S.-W. Cheng, D.-Y. Chiou, Y.-Y. Lai, R.-H. Yu, C.-H. Lee, Y.-J. Cheng, *Org. Lett.* **2013**, *15*, 5338.

[13] a) S. Mataka, K. Takahashi, Y. Ikezaki, T. Hatta, A. Tori, M. Tashiro, *Bull. Chem. Soc. Jpn.* **1991**, *64*, 68; b) M. Wang, X. Hu, P. Liu, W. Li, X. Gong, F. Huang, Y. Cao, *J. Am. Chem. Soc.* **2011**, *133*, 9638; c) I. Osaka, M. Shimawaki, H. Mori, I. Doi, E. Miyazaki, T. Koganezawa, K. Takimiya, *J. Am. Chem. Soc.* **2012**, *134*, 3498; d) K. Kawashima, E. Miyazaki, M. Shimawaki, Y. Inoue, H. Mori, N. Takemura, I. Osaka, K. Takimiya, *Polym. Chem.* **2013**, *4*, 5224.

[14] T. Mori, N. Yana, I. Osaka, K. Takimiya, *Org. Lett.* **2014**, *16*, 1334.

[15] a) E. D. German, A. M. Kuznetsov, *Electrochim. Acta* **1981**, *26*, 1595; b) N. E. Gruhn, D. A. da Silva Filho, T. G. Bill, M. Malagoli, V. Coropceanu, A. Kahn, J.-L. Brédas, *J. Am. Chem. Soc.* **2002**, *124*, 7918; c) D. Moia, V. Vaissier, I. López-Duarte, T. Torres, M. K. Nazeeruddin, B. C. O'Regan, J. Nelson, P. R. F. Barnes, *Chem. Sci.* **2014**, *5*, 281.

[16] a) Z. Xu, L.-M. Chen, G. Yang, C.-H. Huang, J. Hou, Y. Wu, G. Li, C.-S. Hsu, Y. Yang, *Adv. Funct. Mater.* **2009**, *19*, 1227; b) S. K. Hau, H.-L. Yip, N. S. Baek, J. Zou, K. O'Malley, A. K. Y. Jen, *Appl. Phys. Lett.* **2008**, *92*, 253301; c) C.-H. Hsieh, Y.-J. Cheng, P.-J. Li, C.-H. Chen, M. Dubosc, R.-M. Liang, C.-S. Hsu, *J. Am. Chem. Soc.* **2010**, *132*, 4887; d) Y.-J. Cheng, C.-H. Hsieh, Y. He, C.-S. Hsu, Y. Li, *J. Am. Chem. Soc.* **2010**, *132*, 17381.

[17] a) F. Huang, H. Wu, D. Wang, W. Yang, Y. Cao, *Chem. Mater.* **2004**, *16*, 708; b) F. Huang, H. Wu, Y. Cao, *Chem. Soc. Rev.* **2010**, *39*, 2500; c) Z. He, C. Zhong, X. Huang, W. Y. Wong, H. Wu, L. Chen, S. Su, Y. Cao, *Adv. Mater.* **2011**, *23*, 4636; d) Z. He, C. Zhong, S. Su, M. Xu, H. Wu, Y. Cao, *Nat. Photonics* **2012**, *6*, 591; e) C. Duan, K. Zhang, C. Zhong, F. Huang, Y. Cao, *Chem. Soc. Rev.* **2013**, *42*, 9071; f) C. Duan, W. Cai, B. B. Y. Hsu, C. Zhong, K. Zhang, C. Liu, Z. Hu, F. Huang, G. C. Bazan, A. J. Heeger, Y. Cao, *Energy Environ. Sci.* **2013**, *6*, 3022; g) C. Gu, Y. Chen, Z. Zhang, S. Xue, S. Sun, C. Zhong, H. Zhang, Y. Lv, F. Li, F. Huang, Y. Ma, *Adv. Energy Mater.* **2014**, *4*, 1301771; h) G. Long, X. Wan, B. Kan, Z. Hu, X. Yang, Y. Zhang, M. Zhang, H. Wu, F. Huang, S. Su, Y. Cao, Y. Chen, *ChemSusChem* **2014**, *7*, 2358; i) C.-C. Chueh, C.-Z. Li, A. K.-Y. Jen, *Energy Environ. Sci.* **2015**, *8*, 1160.